

Nanomechanical Studies of Superlubricity

Naruo Sasaki*, Noriaki Itamura*, Daisuke Tsuda[#] and Kouji Miura[#]

*Department of Materials and Life Science, Faculty of Science and Technology, Seikei University, Kichijoji Kitamachi 3-3-1, Musashino-shi, Tokyo 180-8633, Japan

[#]Department of Physics, Aichi University of Education, Hirosawa 1, Igayacho, Kariya 448-8542, Japan

Abstract: We briefly review the nanomechanical studies of ultralow friction in the following carbon hybrid systems: atomic force microscopy (AFM) tip on graphite surface, AFM tip on C₆₀/graphite, graphite on graphite surface, graphite/C₆₀/graphite, and C₆₀ intercalated graphite. For the atomic and flake frictions, frictional force maps are compared between simulations and experiments, which can be explained by stick-slip motion of the tip apex atom and flake. For the graphite/C₆₀/graphite system, superlubricity appears, where the maximum static frictional forces have finite values but denote that dynamical frictional forces are zero within the resolution of the experiment. Furthermore, for the C₆₀ intercalated graphite system, greater superlubricity appears. It is clarified that fullerene intercalated graphite films exhibit ultralow average friction force, and excellent friction coefficients $\mu < 0.001$. Our results propose one of the simple guidelines of designing a practical superlubric system – reduction of the contact area between intercalated C₆₀ and graphite sheet to the point contact. Clearly, the C₆₀ intercalated graphite system will contribute to solving energy and environmental problems in the future.

1. INTRODUCTION

It is the ultimate goal of tribology researchers to realize an ideal friction-free machinery system with zero energy consumption. Since the proposal of the concept of an ideal frictionless sliding [1], fundamental studies on superlubricity have been carried based on mainly two different mechanisms, incommensurate contact [2-6] and weak interfacial interaction [7-9]. However, there have been very few studies the aims of which are for practical use in lubrication engineering.

Furthermore, although it can be also expected that graphite intercalated compounds (GIC) are suitable for superlubricants, little work has been done to use GICs as practical lubricants. Therefore we have started to investigate whether GIC is one of the best superlubricants or not. Recently we have shown that a C₆₀ monolayer system confined by graphite walls exhibits superlubricity, ultralow spatial-average friction [10-11]. However it is difficult to construct this system experimentally. Recently we have successfully shown that a C₆₀ intercalated graphite film prepared by chemical and thermal treatments exhibits excellent superlubricity with a low friction coefficient $\mu < 0.001$, which is smaller than $\mu < 0.002$ for MoS₂ [4] and $\mu \cong 0.001$ for graphite [5].

Therefore, in this paper, we systematically discuss frictional properties occurring in atomic-force microscopy (AFM) tip on graphite system, the AFM tip on C₆₀/graphite system, the graphite flake on graphite system, the graphite/C₆₀/graphite system, and the C₆₀ intercalated

graphite system. Several possible mechanisms to induce superlubricity of C₆₀ intercalated graphite system are proposed and discussed. It can be expected that the superlubricity is induced by internal sliding between close-packed C₆₀ monolayers and graphite layers. Our results propose a simple guideline for designing practical superlubric system – reduction of the contact area between intercalated C₆₀ and graphite sheet to the point contact. We anticipate our novel lubrication system to be a starting point for developing more practical superlubricants using intercalated graphite, which will contribute to solving the energy and environmental problems.

2. METHOD

2.1. Experiment

A graphite substrate was prepared by cleaving highly oriented pyrolytic graphite (HOPG). The C₆₀ films on HOPG were prepared by evaporation from a BN crucible. The substrate temperatures during evaporation were kept in the range of 150°C to 200°C. A cleaved graphite flake with an area of 1 mm² and a thickness of about 5 μm was used. A manipulator was used to place a graphite flake on a suitable location on the fixed C₆₀ films/graphite, and thereafter, a rectangular silicon cantilever with a normal spring constant of 0.75 N/m was placed on the graphite flake on the C₆₀ films/graphite using the coordinate data of C₆₀ films/graphite within an experimental error of 0.1 μm [12]. Normal and lateral forces were measured simultaneously under humidity-controlled conditions at room temperature using a commercially available instrument (Seiko instruments Inc., SPI-3700 and Digital instruments Inc., Multi-mode SPM). The scan speed was 0.13 μm/s. Zero normal force was defined as the position at which the cantilever was not bent. The frictional forces were calibrated using the method presented in previous papers [13-15].

*Address correspondence to this author at the Department of Materials and Life Science, Faculty of Science and Technology, Seikei University, Kichijoji Kitamachi 3-3-1, Musashino-shi, Tokyo 180-8633, Japan; Tel: +81-422-37-3777; Fax: +81-422-37-3777; E-mail: naru@st.seikei.ac.jp

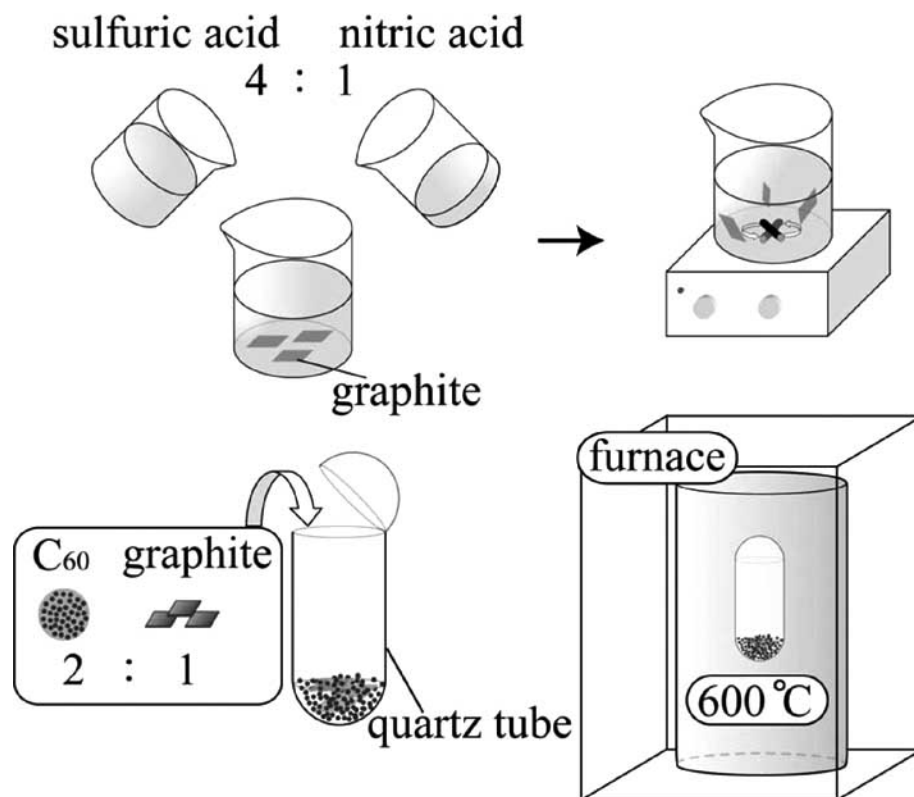


Fig. (1). Preparation of C₆₀ intercalated graphite films.

C₆₀ intercalated graphite films were prepared as illustrated in Fig. 1. Graphite (highly oriented pyrolytic graphite: HOPG) for frictional force measurement and natural graphite powder for high-resolution transmission electron microscopy (HRTEM) were stirred for 16 hours in a reaction mixture of concentrated sulfuric acid and nitric acid (4:1, v/v). The acid-treated natural graphite was washed with water until neutralized and dried at 100°C to remove any remaining water. The dried graphite particles were heat-treated at 1050°C for 15 seconds to obtain exfoliated graphite particles, which were then immersed in 70% alcohol solution in an ultrasonic bath [16-18]. A C₆₀ powder and the exfoliated graphite enclosed in a vacuum-sealed quartz tube were placed in a furnace at 600°C for 15 days [18]. The structure of the C₆₀ intercalated graphite film was investigated using HRTEM (JEM-2000EX) for very thin sections of an intercalated graphite film prepared from natural graphite powder, which is not representative of the entire sample. Friction forces were measured at room temperature using the same instruments mentioned above for an intercalated graphite block prepared from the HOPG.

2.2. Simulation

The simulation for the single-atom friction was performed by the single-atom tip connected to the cantilever spring scanned on a graphite monolayer surface. The model of the graphite monolayer surface consists of 600 carbon atoms and 271 hexagons. The lattice constant of graphite is assumed to be 1.421Å. The details of the model have been already described by Sasaki *et al.* [19-21].

3. SINGLE-ATOM TIP ON GRAPHITE SYSTEM

Fig. 2 shows topographs (atomic force microscope images) of graphite (area S_A), C₆₀ monolayers on graphite (area S_B) and C₆₀ bilayers on graphite (area S_C), obtained by atomic force microscopy.

As shown in Fig. 3A, frictional force maps for graphite (A) show that the tip exhibits one-dimensional stick-slip and

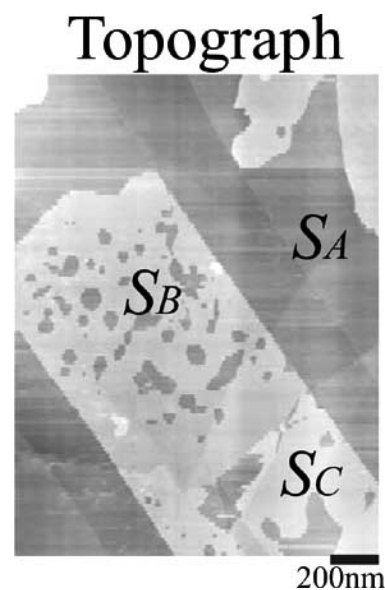


Fig. (2). Topographs (atomic force microscope images) of graphite (area S_A), C₆₀ monolayers on graphite (area S_B) and C₆₀ bilayers on graphite (area S_C).

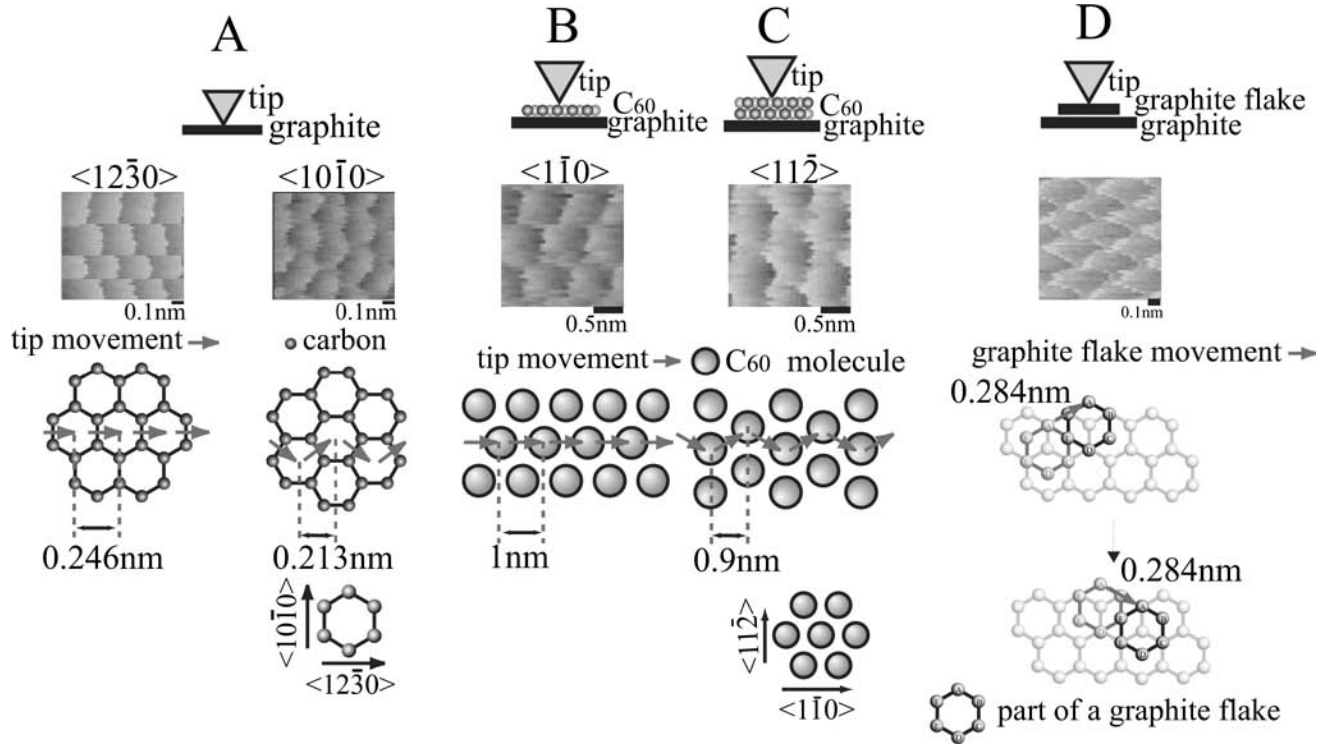


Fig. (3). Frictional force maps and tip movements for representative scan directions for graphite (A), C_{60} monolayers on graphite (B), and C_{60} bilayers on graphite (C). Frictional force map and flake movement of graphite flake on graphite (D). Frictional force maps and tip movements for (B) and (C) are the same.

two-dimensional zigzag stick-slip motions for $[12\bar{3}0]$ and $[10\bar{1}0]$ scanning directions, respectively [5,19-23], although they exhibit significant load dependence at small loads [5,21,23] as shown in Fig. 4. Fig. 4 shows the experimental and simulated frictional force maps scanned along $[1230]$ directions for two different loading forces. It can be seen clearly that the experimental image patterns are in very good agreement with the simulated ones, and change significantly depending on the load. At a lower loading force, the zigzag pattern corresponding to the C-C bond of the graphite lattice appears. However, as the load increases, this zigzag pattern vanishes and only the straight pattern parallel to the scan direction appears. The experimental loading force for measuring frictional force image patterns in our experiment is much smaller than that reported by Fujisawa *et al.* [23]. The reason for this difference is ascribed to the effect of water covering the graphite surface [5], which can be explained as follows: Since our experiment is performed under ambient conditions, where the relative humidity is around 50%, a long-range capillary force, F_{cap} , is dominant as a tip-surface interaction force. In this case, the water meniscus is formed between the tip and graphite surface as shown in the inset of Fig. 4, which produces the attractive capillary force such as

$$F_{\text{cap}} = -\frac{4\pi\gamma R \cos\theta}{1+z/R(1-\cos\phi)},$$

where z is the tip-to-surface distance, R is the radius of curvature of the tip of the atomic force microscope, θ and ϕ are the contact and meniscus angles, respectively [24], and

$\gamma = 0.07$ N/m is the surface tension of water. In the case of $R=20$ nm, estimated value of the tip used in our experiment, $\theta = 0$ deg. and $\phi = 10$ deg., the calculated F_{cap} for the tip height $z=0.2$ nm is about -11 nN, corresponding well to pull-off forces $F_{\text{pull-off}} \approx -8$ nN measured in our present experiment. Thus F_{cap} significantly contributes to the total loading force in our experiment, which produces a difference from the previously observed loads [20,21,23] and from ours.

4. SINGLE-ATOM TIP ON C_{60} /GRAPHITE SYSTEM

As shown in Figs. 3B and 3C, frictional force maps for B and C show that the tip exhibits one-dimensional stick-slip and two-dimensional stick-slip motions for the $[1100]$ and $[112]$ scanning directions of a $C_{60}(111)$ surface, respectively [14,15]. The frictional force maps for B show that the C_{60} monolayer consists of close-packed C_{60} molecules.

5. GRAPHITE FLAKE ON GRAPHITE SYSTEM

When a graphite flake is placed on areas S_A of Fig. 2, the graphite flake on the graphite (which we call graphite/graphite: D) is obtained. The frictional force map for Fig. 3D shows that the graphite flake moves on the graphite such that the AB stacking of the graphite is maintained [5]. The movement of the flake on the graphite surface can be converted to the movement of a center of the flake mass with a constant velocity in the effective potential as follows:

$$V = V_0 \left\{ 2 \cos\left(\frac{2\pi}{a}x\right) \cos\left(\frac{2\pi}{a\sqrt{3}}y\right) + \cos\left(\frac{4\pi}{a\sqrt{3}}y\right) \right\},$$

where $a=0.142\text{ nm}\times 2 = 0.284\text{ nm}$. This effective potential is determined so that it takes the minimum values at the natural stacking position of the graphite as shown in Fig. 5(a). This simple preliminary simulation reproduces experimental frictional-force images quite well, as shown in Fig. 5(b). Here, the spacing of $a = 0.284\text{ nm}$ indicates a distance from the present to the next stable position so that AB stacking of the graphite is held.

A more detailed numerical simulation of flake dynamics was performed by Matsushita *et al.* [25]. It is shown that the

stick-slip motion of the flake is due to the binding of the flake close to AB stacking configurations of the graphite substrate.

6. GRAPHITE/C₆₀/GRAPHITE SYSTEM

When a graphite flake is placed on areas S_B of Fig. 2, the graphite flake on the C₆₀ monolayer/graphite (which we call graphite/C₆₀/graphite: E) is obtained. Figure 6 shows frictional force maps as a function of loading force for the graphite/C₆₀/graphite (E). The patterns of maps E show

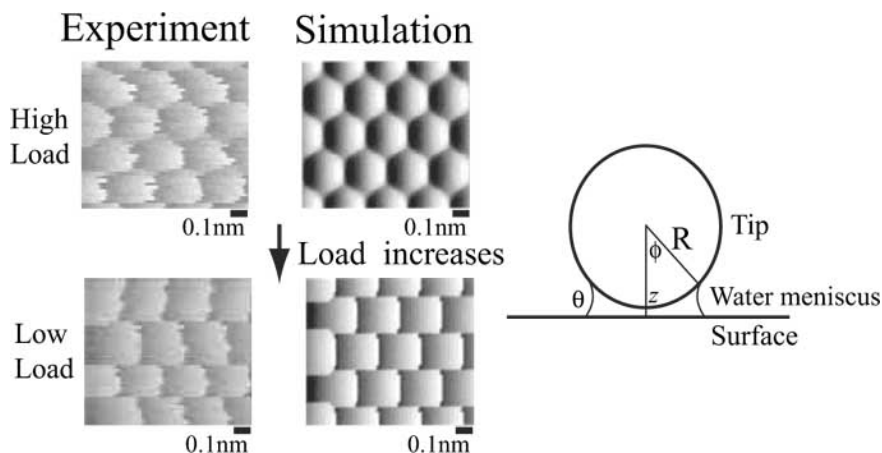


Fig. (4). Experimental and simulated frictional maps of graphite at two different loading forces for the single-atom tip scanned on the graphite. The inset shows the water meniscus formed between the tip and graphite surface.

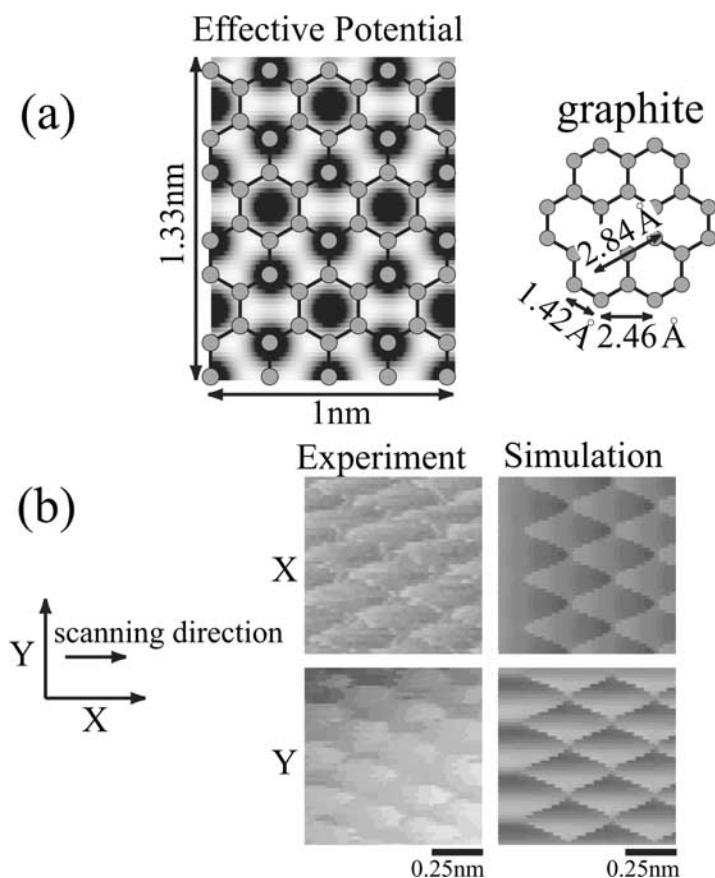


Fig. (5). (a) Effective potential of a graphite flake on the graphite surface. (b) Comparison between experimental images and simulated ones, for the flake scanned on the graphite.

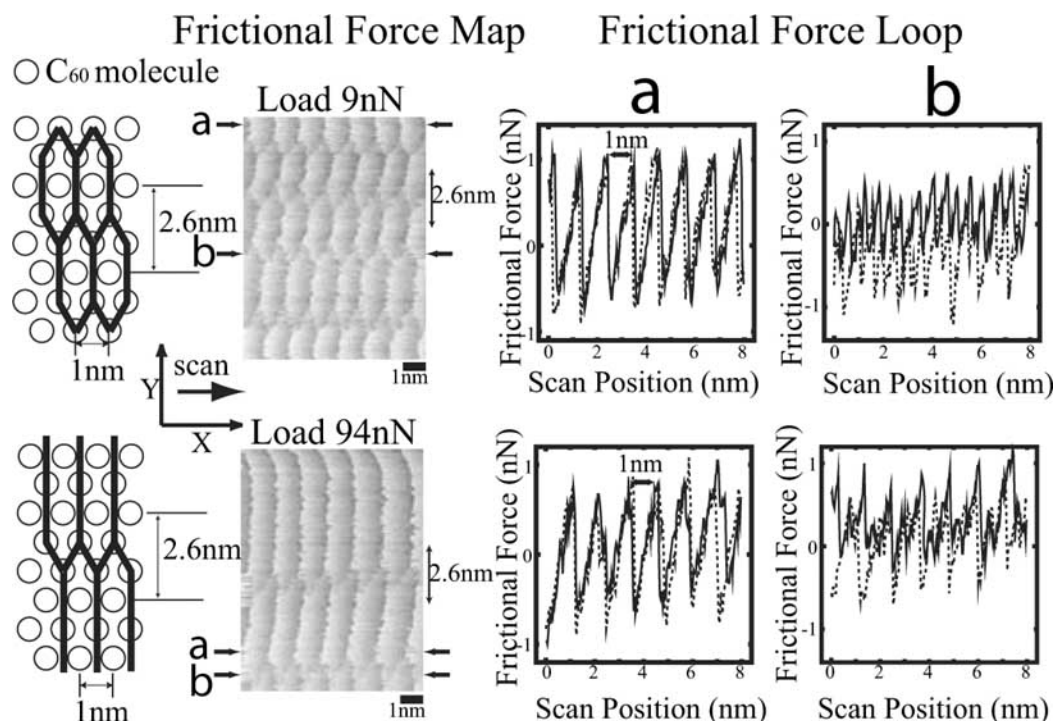


Fig. (6). Frictional force maps versus loading force (9 and 94 nN) for graphite/ C_{60} /graphite (E). Frictional force loops obtained from line profiles indicated by arrows *a* and *b* in the frictional force maps are also represented, where the solid and broken lines indicate one direction and in the opposite direction, respectively.

transitions depending on the load, and eventually exhibit chainlike ones as shown in Fig. 6. Here, it should be noted that the maps E are composed of friction between a tip and a graphite flake, and that between a C_{60} monolayer and two graphite plates. However, they are completely clearly different from those obtained for graphite(A) [5,19-23], from the standpoint of periodic pattern and contrast, as shown in Fig. 3D and Fig. 5. This denotes that the friction between the tip and the graphite flake is greater than that between the C_{60} monolayer and two graphite plates, which denotes that the graphite flake moves together with the tip during a scan. The frictional force map at a load of 9 nN has a periodicity of 1 nm along the *x*-direction (scan direction), which reflects the close-packed C_{60} molecular arrangement, as shown in Fig. 6. However, it has a periodicity of 2.6 nm along the *y*-direction, vertical to scan direction, which shows a super cell structure.

Here, it should be noted that the frictional loops obtained from line profiles (solid and dotted sawtooth lines) indicated by arrow *a* in the frictional force maps E do not exhibit hysteresis, which indicates that the mean frictional forces are zero and thus there is no energy dissipation [26]. As shown on the bottom of Fig. 6, the mean frictional forces at the position *a* are zero up to a high load, although the frictional forces have a finite value. On the other hand, those shown by arrow *b* show some hysteresis with energy dissipation, in which two-dimensional zigzag motions of a graphite flake occur. Furthermore, Fig. 6 shows that unit cells of frictional force maps become enlarged along the *y* direction, as the loading force increases from 9 nN to 94 nN, which denotes that the region where the mean frictional force is zero, as indicated by arrow *a*, becomes larger as the load increases. Therefore the region for superlubricity increases as the

load increases, which is useful for industrial application as a lubricant. The load dependence of dynamic frictional force is shown in Fig. 7. The maximum frictional force in this experiment is estimated to be below 1 nN, which is comparable to the shear force (0.4 nN) between a single C_{60} single molecule and graphite [15]. In the case of more than two layers of C_{60} molecules, the observed frictional forces rapidly increase due to elastic properties of solid C_{60} crystals, which no longer leads to the low frictional features mentioned above.

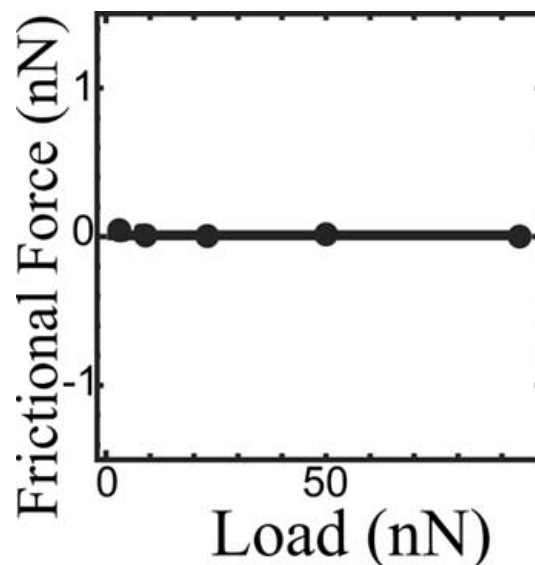


Fig. (7). Mean frictional forces versus loading force indicated by the arrow *a* in Fig. 6.

It can be expected that the superlubric feature of lateral force curves without hysteresis is due to, for example, rolling dynamics of each C_{60} molecule as shown in Fig. 8, which can be called the “picture of single-molecular bearing”. However, as the number of C_{60} molecules adsorbed on the graphite is increased, the interaction between C_{60} molecules cannot be neglected any longer. Recent micro canonical molecular dynamics calculation by Legoas *et al.* [27] has showed that the C_{60} molecule is adsorbed on the graphite surface forming the “frustrated AB stacking structure”, and, under a certain condition, each C_{60} molecule fluctuates around the equilibrium position. Thus recent simulations [27-28] have shown that dynamics of C_{60} molecules exhibit much more complicated features than the picture of the single molecular bearing.

7. C_{60} INTERCALATED GRAPHITE SYSTEM

7.1. Structure - Experiment and Theory

HRTEM images of the C_{60} intercalated graphite thin film (mean diameter: 500 μm) are shown in Figs. 9(a) and 9(b), normal to the (0001) plane of graphite and parallel to the (0001) plane of graphite, respectively, where the indexes used are the same as those of graphite. These images show that the close-packed C_{60} monolayers of the nearest neighbour distance 1nm between C_{60} molecules within the (0001) plane of graphite, are formed with a periodic spacing of 1.3nm normal to the (0001) plane of graphite. The interlayer spacing of 1.3nm can be reproduced by simulation as follows: Figure 9(c) shows a model for calculating the equilibrium distance d of C_{60} monolayer intercalated between graphite sheets. The normal load F_2 and total energy U as functions of distance between graphite sheets d were

calculated optimizing the structure of graphite/ C_{60} /graphite system, using the Tersoff potential [29] as a potential energy of chemical bonds within C_{60} molecules, and the modified Lennard-Jones potential [30,31] as an interaction potential energy between C_{60} molecules and graphite sheets. For $d \cong 1.31\text{nm}$, $F_2 = 0$ (U takes a minimum value), which means that $d \cong 1.31\text{nm}$ is an equilibrium distance as shown in Fig. 9(d). However it should be noted again that, HRTEM images were taken on very thin sections, and may not be representative of the entire sample. Therefore in the newly developed sample, close-packed C_{60} monolayers and graphite layers are not necessarily periodically repeated as shown in Fig. 9(b), which will be discussed below.

Furthermore, HRTEM images of the fullerene intercalated graphite film quite often have moiré features, which exhibits that fullerene close-packed monolayers have orientations around the c-axis of the graphite slightly different from each other. When the C_{60} close-packed monolayers distribute randomly around the c-axis of the film, ultralow friction is expected to be observed in all scan directions mentioned below. The essentially same mechanism - friction-induced reorientation of the (0001) basal planes of the MoS_2 grains - has been already pointed out by Martin *et al.* [4].

7.2. Frictional Properties

Fig. 10 shows the lateral force versus displacement hysteresis loops for the C_{60} intercalated graphite film (2.3mmx2.3mmx0.2mm) using a frictional force microscope. When the loading force is lower than 100nN, the friction forces are not periodic and becomes ultralow with less than the order of 0.1nN. Furthermore, the feature of ultralow

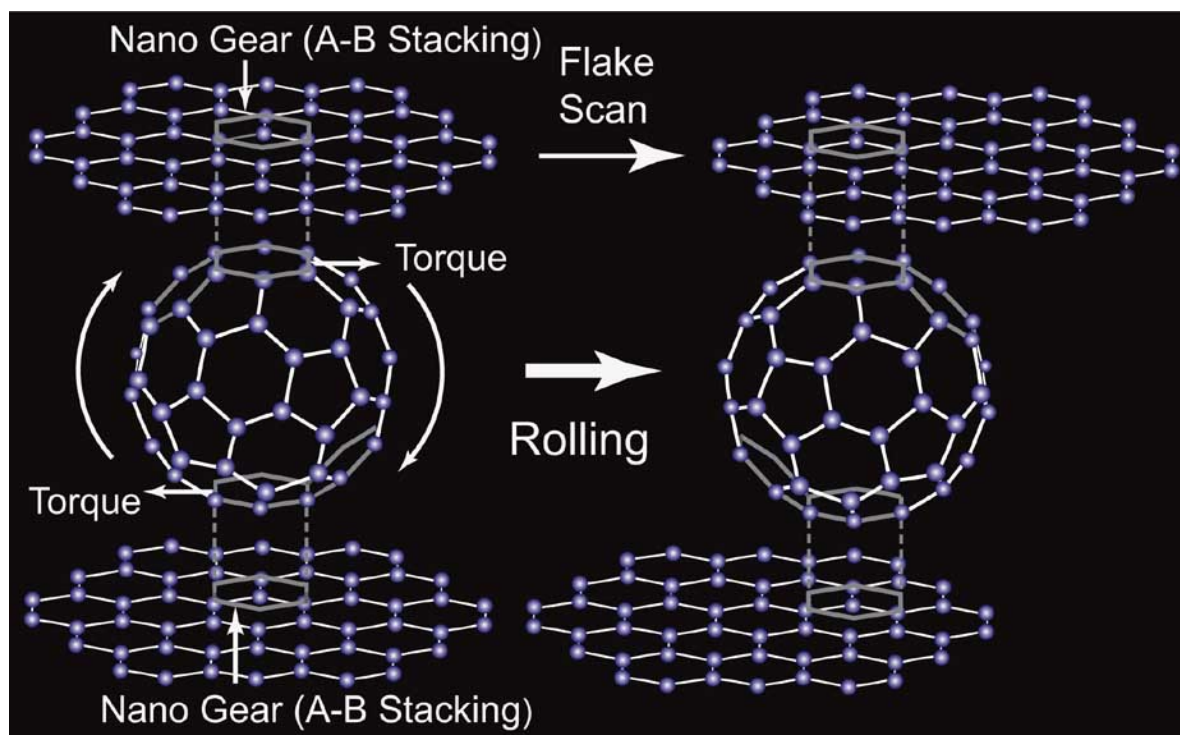


Fig. (8). Picture of “single molecular bearing”: For example, C_{60} molecule rolls by means of torque, which is produced by the nano-gears of six-membered rings between C_{60} molecules and the upper and lower graphite plates.

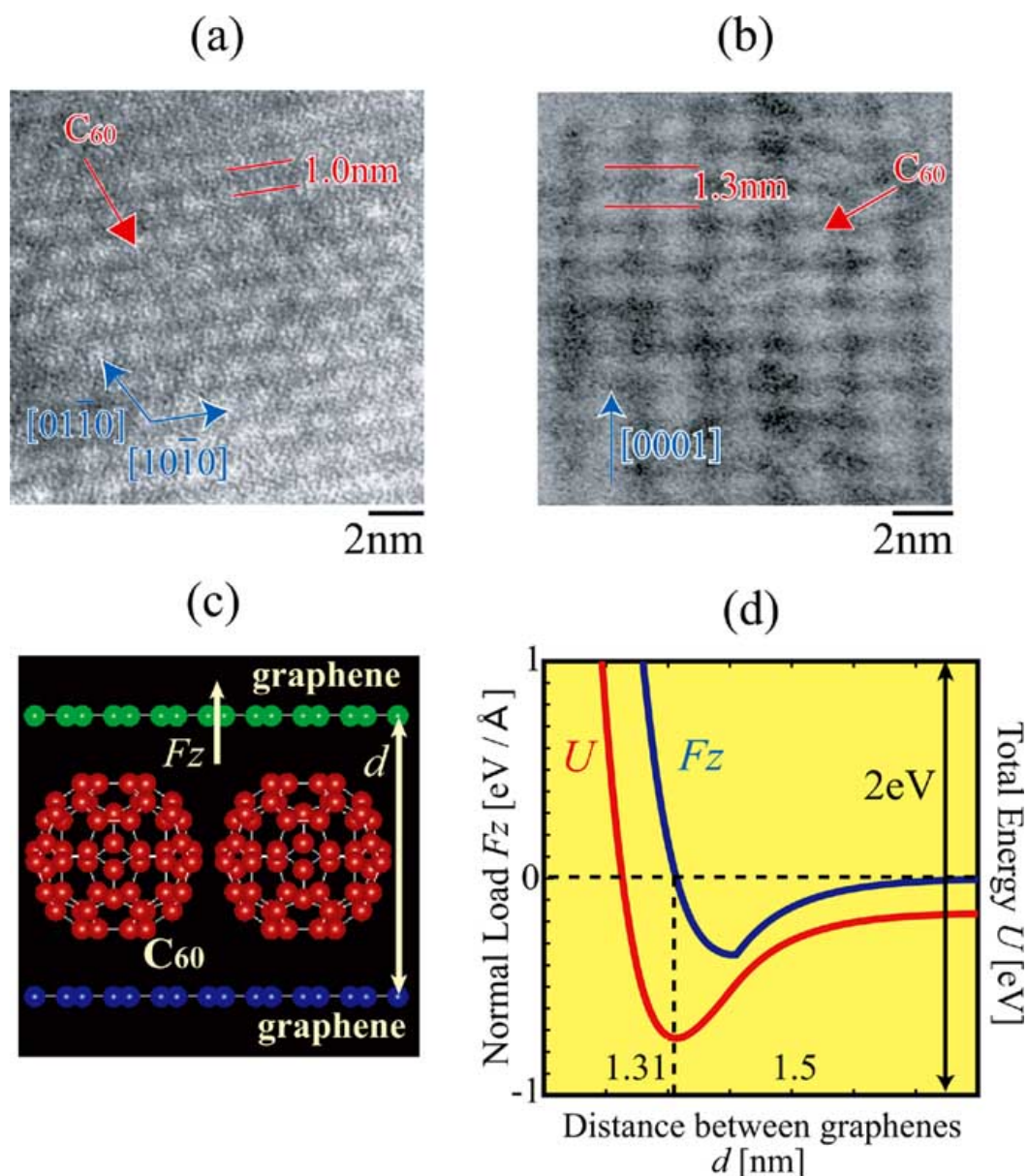


Fig. (9). (a) and (b) High-resolution transmission electron microscopy (HRTEM) images of C_{60} intercalated graphite film, normal to (0001) plane of graphite and parallel to (0001) plane of graphite, respectively, where indexes of this film used are the same as those of graphite. (c) Model for calculating equilibrium distance d of graphite/ C_{60} monolayer/graphite sandwiched system. Normal load F_z and total energy U as functions of graphite interlayer distance d . For $d \cong 1.31$ nm, $F_z = 0$ (U takes a minimum value), which means that $d \cong 1.31$ nm is an equilibrium distance.

friction force was observed in all scan directions, which is confirmed by rotating the scanner underneath the C_{60} intercalated graphite substrate. The relation between the mean lateral force $\langle F_L \rangle$ and the load F_z exhibits friction coefficient $\mu < 0.001$ which is smaller than $\mu < 0.002$ for MoS_2 observed by Martin *et al.* [4] and $\mu \cong 0.001$ for graphite previously observed by our group [5].

However the loading force increases up to nearly 100 nN, which we call the critical loading force, the lateral pattern with 1-nm-period spacing appears, which corresponds to the nearest neighbor spacing between C_{60} molecules within a C_{60} close-packed monolayer but not to that between the carbon atoms of the graphite. The critical loading force ranges from

80 nN to 120 nN over the entire surface of film. This result indicates the possibility that the motion of C_{60} molecules is inhibited by the squeezing action of graphite walls and/or by the formation of a chemical bond between a C_{60} molecule and a graphene [32]. This speculation also indicates that an existence of fluid layers confined by solid surface would be important for smooth sliding of graphite sheet, which must be further studied both theoretically and experimentally.

7.3. Structural Model

The structure of the C_{60} intercalated graphite film is discussed. First we consider the validity of the simple assumption that a C_{60} intercalated graphite film is comprised

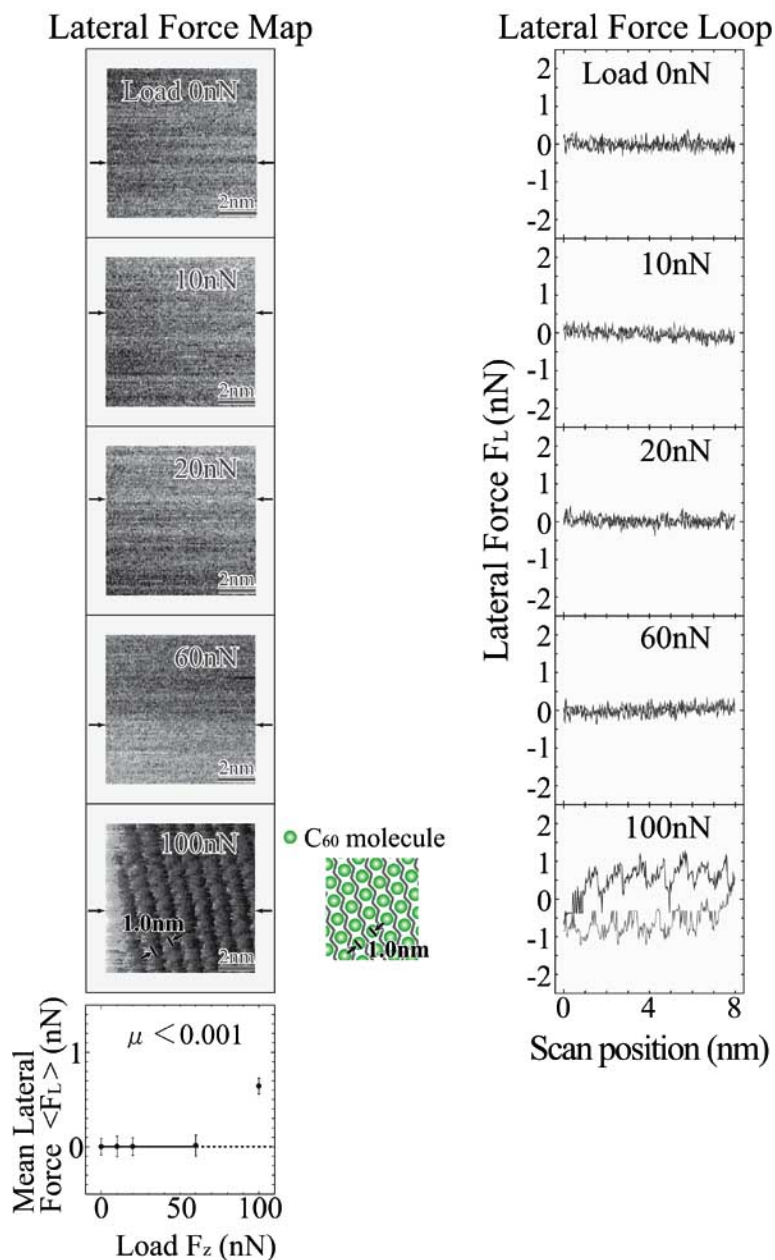
C₆₀ Intercalated Graphite Film

Fig. (10). Lateral force maps and lateral force hysteresis loops as a function of displacement for a C₆₀ intercalated graphite film obtained using a frictional force microscope, where the black and grey-colored lines indicate one direction and its opposite, respectively. At a loading force of 100 nN, the lateral pattern with 1-nm-period spacing appears, which corresponds to the nearest neighbor spacing between C₆₀ molecules within a C₆₀ close-packed monolayer but not to that between the carbon atoms of the graphite.

of $n+1$ parallel layers, which can be modelled by the series connection of the n lateral springs as illustrated in Fig. 11. If the unit structures of graphite sheet and C₆₀ monolayer repeat periodically, n is evaluated as $n=0.2\text{mm}(\text{sample thickness})/1.3\text{nm}(\text{interlayer distance}) \cong 1.5 \times 10^5$. Furthermore, the effective spring constant of each lateral spring which corresponds to that of graphite/C₆₀/graphite layer, is obtained as $k \approx 1\text{N/m}$ according to our previous measurement of graphite/C₆₀/graphite system [10], since the lateral force curve for a graphite/C₆₀/graphite system measured by our group shows sawtooth behavior with a magnitude on the

order of 1 nN for a period of 1nm^{10} . Therefore, if it is assumed that the shear force is uniformly spread on the C₆₀ intercalated graphite film, the effective spring constant of the series connection of the n lateral springs becomes $k_{\text{eff}} \approx 1/n$ N/m. Here it should be noted that the lateral force of 0.1 nN observed in our experiment induces the macroscopic lateral deflection of the top layer of graphite sheet or the scan length of $l = 0.1 \times n$ nm. If $n \cong 1.5 \times 10^5$ is substituted, $l = 0.1 \times n \cong 15\mu\text{m}$ is obtained. This means that the series connection of the n lateral springs elastically deforms during the scan length of $15\mu\text{m}$.

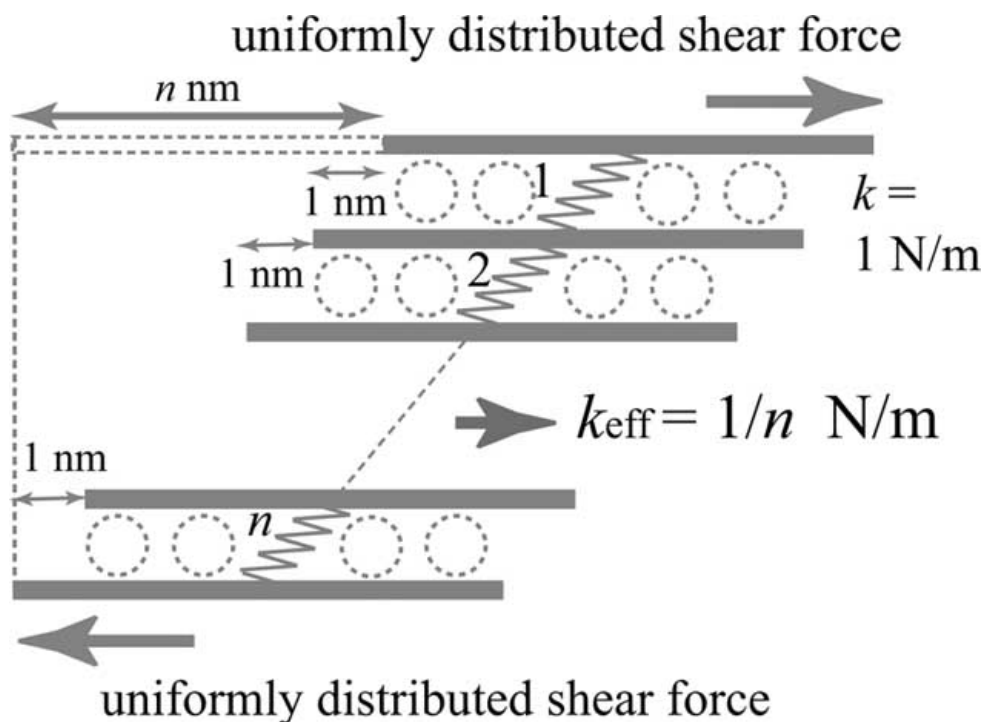


Fig. (11). If it is assumed that the shear force is uniformly spread on the C_{60} intercalated graphite film, C_{60} intercalated graphite film comprised of n parallel layers of graphite and C_{60} monolayer, can be modelled by the series connection of the n lateral springs.

However we must be careful to conclude here only by this simple elastic model because it seems difficult to determine whether the scan process shown in Fig. 10 is within the elastic region or not, due to our limited noise level of 0.1nN, even if the tip is moved far around 15 μm . Furthermore our preliminary simulations of the graphite/ C_{60} /graphite system and the previous simulations by other groups [27-28] have shown that stick-slip sliding of the graphite sheet occurs even on an atomic scale, and that the periodic friction force of several piconewtons with a periodicity of the order of 1nm is obtained, which indicates the elastic region is less than 1nm. Thus considering the behaviour on atomic scale, $n \cong 10$ is obtained from $l = 0.1 \times n \cong \text{nm}$, which is quite different from the above simple evaluation $n \cong 1.5 \times 10^5$.

This significant difference of evaluation of n is due to the following possible reasons: First, there is a possibility that only small parts of the gap between graphite sheets are packed by C_{60} molecules as shown in Fig. 12(a). Second, the shear force is not actually distributed uniformly due to the finite elastic contact radius between the tip and the surface. Third, the composite is comprised of a nonuniform layered structure such as domains and island structures. These problems can be clarified by obtaining the lateral force curve with a scan length of more than μm using friction force microscopy or by measuring the friction using a larger tip with a radius of curvature of more than one μm . In both cases high sensitivity which can measure the friction coefficient of less than 0.001 is required. This kind of study is very important to clarify the mechanism of friction on the intermediate scale between nm and mm, and the relation between the nanotribology and macrotribology, which is closely related to hierarchy of friction.

7.4. Guideline for Designing Superlubric System

Our results demonstrate a simple guidelines for designing practical superlubric system. In the case of the graphite system, the surface contacts (gray-colored regions) are formed between graphite sheets as illustrated in Fig. 13(a). On the other hand, in the case of our fullerene intercalated graphite system, the contact area (gray-colored regions) between fullerene molecules and graphite sheets is remarkably reduced as shown in Fig. 13(b). Here, if it is assumed that each contact area between fullerene and graphite is approximately the same size as the rhombic-shaped area within the unit cell of the graphite, the force required to slide the upper graphite sheet for the fullerene intercalated graphite (Fig. 13(b)) can be qualitatively evaluated as only several percents of that for the graphite (Fig. 13(a)), because of $(a_2/a_1)^2 \cong 0.06$, where a_1 and a_2 denote the lengths of one side of the unit cells of the graphite and the C_{60} intercalated graphite, respectively (Figs. 13(a) and 13(b)). Of course it can be expected that the superlubric feature decreases when the contact area increases due to the deformation of fullerene for the large loading force. This superlubric mechanism derived from the reduction of the contact area works well because of the weak van der Waals interaction force acting between the C_{60} molecule and the graphite sheet. However, in the case of the C_{60} adsorbed silicon and the metal intercalated graphite, strong chemical bonds are formed, which prevents the graphite sheet sliding smoothly. Thus we think the reduction of the contact area in the system comprised of inert carbon materials is one of the main reasons that our newly developed C_{60} intercalated graphite exhibits much more excellent superlubric properties than conventional lubricants, and that internal sliding mainly occurs between graphite sheet and fullerene monolayer.

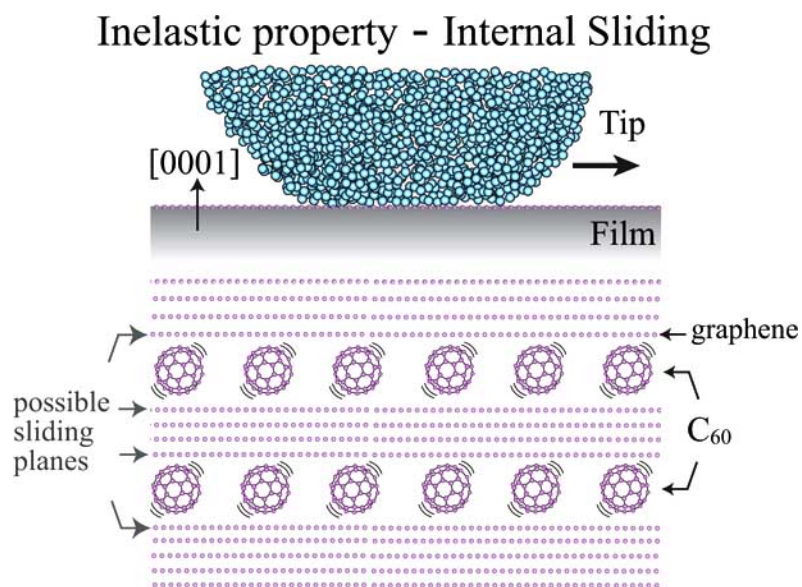


Fig. (12). Structural model of C_{60} intercalated graphite films consisting of close-packed C_{60} monolayers and graphite layers with 1.3-nm-period spacing. The film slides mainly between each C_{60} monolayer and graphene indicated by arrows.

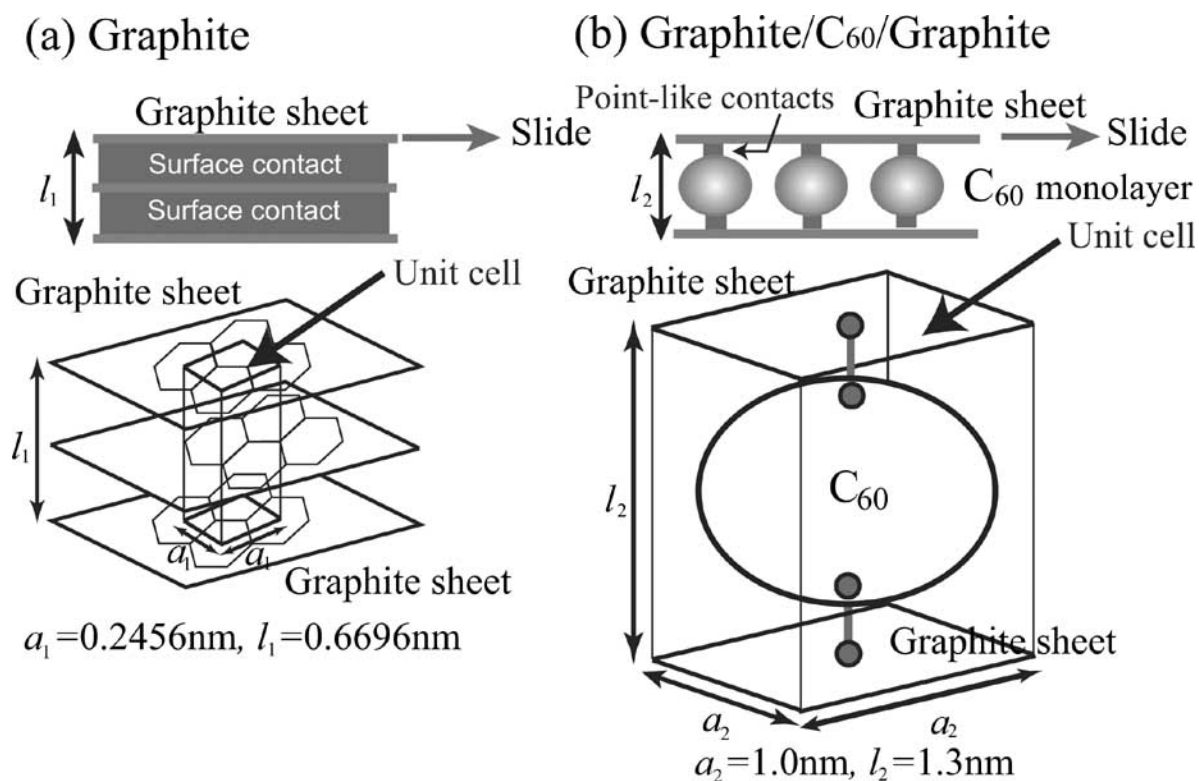


Fig. (13). (a) In the graphite system, the “surface contacts” are formed between graphite sheets. (b) In the C_{60} intercalated graphite system, the surface contacts between C_{60} molecules and graphite sheets are remarkably reduced to “point contacts”.

Furthermore the important point of our system is that this point-contact type bonds between C_{60} and graphite are not only weak enough to move C_{60} molecules smoothly as molecular bearings, but also strong enough to hold the C_{60} intercalated graphite structures firmly. Therefore C_{60} intercalated graphite structure, especially that for C_{60} , can be considered as one of the best carbon composites to achieve superlubricity.

CONCLUSION

In this paper, we have reviewed the mechanism of the friction of the following system; AFM tip on the graphite surface, AFM tip on C_{60} /graphite, graphite on graphite surface, graphite/ C_{60} /graphite, and C_{60} intercalated graphite. For the atomic friction, frictional force maps significantly change at extremely small loads, which can be explained by

the change of stick-slip motion of the tip apex atom. For the flake friction, the graphite flake moves on the graphite surface such that the stacking of graphite layers is maintained. For the graphite/C₆₀/graphite system, the maximum static frictional forces have finite values but denote that dynamical frictional forces are zero within the resolution of the experiment. In order to explain the mechanism of superlubricity, the picture of "single molecular bearing" is proposed.

Finally, for the C₆₀ intercalated graphite system, both the maximum static frictional forces and the dynamical frictional forces are zero within the resolution of the experiment. The novelty or superiority of the C₆₀ intercalated graphite system compared to the previous works on superlubricity demonstrates a guideline for designing practical superlubric systems, to develop practical fullerene intercalated graphite lubricants according to this guideline, and to control superlubric properties of this system. From the standpoints of technology, our novel system is a starting point for developing more practical and effective superlubricants using intercalated graphite, which will contribute to reducing the energy loss and the increase of durability, and solving eventually energy and environmental problems.

ACKNOWLEDGEMENTS

This research was supported by a Grant-in-Aid for Scientific Research from the Ministry of Education, Culture, Sports, Science and Technology (No.16340089, No. 17760030, and No.18340087) and by "Practical Application Research, Science and Technology Incubation Program in Advanced Regions," JST. We are also thankful for the financial support provided by the "High-Tech Research Center" Project for Private Universities. One of the authors (N.S.) acknowledges the financial support provided by "Organization and Functions," PRESTO-JST."

REFERENCES

- [1] McClelland, G. Friction at weakly interacting interfaces, in *Adhesion and Friction*, edited by M. Grunze and H. Kreuzer, Springer-Verlag, Berlin, **1989**, 1.
- [2] Hirano, M.; Shinjo, K. *Phys. Rev. Lett.* **1991**, *67*, 2642.
- [3] Hirano, M.; Shinjo, K.; Kaneko, R.; Murata, Y. *Phys. Rev. Lett.* **1997**, *78*, 1448.
- [4] Martin, J. M.; Donnet, C.; Mogné, L. *Phys. Rev. B* **1993**, *48*, 10583.
- [5] Miura, K.; Sasaki, N.; Kamiya, S.; *Phys. Rev. B* **2004**, *69*, 075420.
- [6] Dienwiebel, M.; Verhoeven, G. S.; Pradeep, N.; Frenken, J. W. M.; Heimberg, J. A.; Zandbergen, H. W. *Phys. Rev. Lett.* **2004**, *92*, 126101.
- [7] Colchero, J.; Marti, O.; Mlynek, J. Friction on an atomic scale, in *Forces in Scanning Probe Methods*, ed. by H.-J. Guntherodt et al. Kluwer Academic Publishers, Netherlands, **1995**.
- [8] Sasaki, N.; Kobayashi, K.; Tsukada, M. *Phys. Rev., B* **1996**, *54*, 2138.
- [9] Socoliuc, A.; Bennewitz, R.; Gnecco, E.; Meyer, E. *Phys. Rev. Lett.* **2004**, *92*, 134301.
- [10] Miura, K.; Kamiya, S.; Sasaki, N. *Phys. Rev. Lett.* **2003**, *90*, 055509.
- [11] Sasaki, N.; Miura, K. *Jpn. J. Appl. Phys.* **2004**, *43*, 4.
- [12] Miura, K.; Kamiya, S. *Europhys. Lett.* **2002**, *58*, 610.
- [13] Miura, K.; Takagi, T.; Kamiya, S.; Sahashi, T.; Yamauchi, M. *Nano Lett.* **2001**, *1*, 161.
- [14] Okita, S.; Ishikawa, M.; Miura, K. *Surf. Sci.* **1999**, *442*, L959.
- [15] Okita, S.; Miura, K. *Nano Lett.* **2001**, *1*, 101.
- [16] Nakajima, T.; Matsuo, Y. *Carbon* **1994**, *32*, 469.
- [17] Chen, G.; Wu, D.; Weng, W.; Wu, C. *Carbon* **2003**, *41*, 579.
- [18] Gupta, V.; Scarf, P.; Rich, K.; Romans, H.; Müller, R. *Solid State Commun.* **2004**, *131*, 153.
- [19] Sasaki, N.; Kobayashi, K.; Tsukada, M. *Phys. Rev. B* **1996**, *54*, 2138.
- [20] Sasaki, N.; Tsukada, M.; Fujisawa, S.; Sugawara, Y.; Morita, S.; Kobayashi, K. *J. Vac. Sci. Technol. B* **1997**, *15*, 1479.
- [21] Sasaki, N.; Tsukada, M.; Fujisawa, S.; Sugawara, Y.; Morita, S.; Kobayashi, K. *Phys. Rev. B* **1998**, *57*, 3785.
- [22] Morita, S.; Scarf, P.; Rich, K.; Sugawara, Y. *Surf. Sci. Rep.* **1996**, *23*, 1.
- [23] Fujisawa, S.; Yokoyama, K.; Sugawara, Y.; Morita, S. *Phys. Rev. B* **1998**, *58*, 4909.
- [24] Israelachvili, J. N. *Intermolecular and Surface Forces*, Academic Press, London **1985**.
- [25] Matsushita, K.; Matsukawa, H.; Sasaki, N. *Solid State Commun.* **2005**, *136*, 51.
- [26] The hysteresis of the piezoactuator is extremely small within a nanometer scan. A trivial change in C₆₀ molecular arrangements between one direction and the opposite direction scanings may occur, which gives the possibility that some hysteresis is produced. However, the quantities of the hysteresis are less than a few percent in this experiment. Hence, it can be concluded that within experimental errors, no hysteresis exists and mean frictional forces are zero.
- [27] Legoas, S. B.; Giro, R. Galvao, D. S. *Chem. Phys. Lett.* **2004**, *386*, 425.
- [28] Kang, J.; Hwang, H. *Nanotechnology* **2004**, *15*, 614.
- [29] Tersoff, J. *Phys. Rev. Lett.* **1988**, *61*, 2879.
- [30] Stoddard, S. D.; Ford, J. *Phys. Rev. A* **1973**, *8*, 1504.
- [31] Lu, J. P.; Li, X. P.; Martin, R. M. *Phys. Rev. Lett.* **1992**, *68*, 1551.
- [32] Wanlin, G.; Zhu, C. Z.; Yu, T. X.; Woo, C. H.; Zhang, B.; Dai, Y. T. *Phys. Rev. Lett.* **2004**, *43*, 245502.